Magnetization dynamics in the normal and superconducting phases of UPd_2Al_3: I. Surveys in reciprocal space using neutron inelastic scattering

2006 J. Phys.: Condens. Matter 18 R437

(http://iopscience.iop.org/0953-8984/18/27/R01)

INSTITUTE OF PHYSICS PUBLISHING JOURNAL OF PHYSICS: CONDENSED MATTER

J. Phys.: Condens. Matter **18** (2006) R437–R451 doi:10.1088/0953-8984/18/27/R01

TOPICAL REVIEW

Magnetization dynamics in the normal and superconducting phases of UPd_2Al_3: I. Surveys in reciprocal space using neutron inelastic scattering

A Hiess[1], N Bernhoeft[2], N Metoki[3], G H Lander[3,4], B Roessli[5], N K Sato[6], N Aso[7], Y Haga[3], Y Koike[3], T Komatsubara[8] and Y Onuki[9]

[1] Institut Laue Langevin, BP 156X, F-38042 Grenoble, France
[2] Départmento de Recherche Fondamentale sur la Matière Condensée, CEA-Grenoble, F-38054 Grenoble, France
[3] Advanced Science Research Centre, Japan Atomic Energy Research Institute, Tokai, Naka, Ibaraki 319-1111, Japan
[4] European Commission, JRC, Institute for Transuranium Elements, Postfach 2340, D-76125 Karlsruhe, Germany
[5] Laboratory for Neutron Scattering, ETH Zurich and Paul Scherrer Institute, CH-5232 Villigen, Switzerland
[6] Department of Physics, Nagoya University, Furo-cho, Chikasu-ku, Nagoya 464-8602, Japan
[7] Neutron Science Laboratory, Institute for Solid State Physics, University of Tokyo, Shirakata 106-1, Tokai-mura, Ibaraki 319-1106, Japan
[8] Physics Department, Graduate School of Science, Tohoku University, Sendai 980-8578, Japan
[9] Graduate School of Science, Osaka University, Toyonaka 560-0043, Japan

Received 31 March 2006
Published 23 June 2006
Online at stacks.iop.org/JPhysCM/18/R437

Abstract

This topical review presents results from neutron inelastic scattering experiments on single crystals of UPd_2Al_3. The focus is on the experimental situation, while the sequel paper advances theoretical perspectives. We present a detailed and complete characterization of the wavevector- and energy-dependent magnetization dynamics in UPd_2Al_3 as measured by neutron inelastic scattering primarily in the form of extensive surveys in energy–momentum space under a wide range of experimental conditions, and put our observations in context with data that has been published previously by two independent groups. In this way we emphasize the robustness of the results, which indicate the intricate nature of the dynamic magnetic susceptibility of this material. This study yields unique insight into the low-temperature ground state, which exhibits a microscopic coexistence of antiferromagnetism and superconductivity, making UPd_2Al_3 one of the most accessible heavy-fermion superconductors that can be fully characterized by neutron spectroscopy.

(Some figures in this article are in colour only in the electronic version)

Contents

1. Introduction

The co-existence of magnetism and superconductivity continues to attract the attention of the condensed matter community. It is of particular interest to establish whether the superconducting state is stabilized via a dynamic deformation of the lattice, magnetic or other electronic potential. For both high-T_c and heavy-fermion superconducting materials, the discussion has been, and still is, extremely controversial. Three fundamental questions arise. First, is it meaningful to discuss superconductivity and magnetism as two separate phenomena or are they joint manifestations of a novel low-temperature ground state? Second, on assuming that some reduction of the two aspects may be made, what are the symmetries of the order parameters? Finally, can one identify coupling mechanisms that maintain the broken symmetry of the appropriate wavefunction?

Of the materials that are known to exhibit both ordered magnetism and superconductivity, the compound UPd_2Al_3 occupies an especially interesting place. Initially investigated by Geibel and collaborators [1], it has the following favourable properties: first, a simple atomic structure, hexagonal space group $P6/mmm$ ($a = 5.350$ Å, $c = 4.185$ Å), and the possibility of growing stoichiometric, bulk superconducting single crystals of ∼2–3 g; second, a simple antiferromagnetic structure, $T_N = 14.3$ K, with ferromagnetic sheets of uranium moments parallel to [1 0 0] stacked in alternating directions along the hexagonal **c**-axis (see figure 1), giving an antiferromagnetic wavevector $\mathbf{Q}_0 = (0\ 0\ 1/2)$ reciprocal lattice units (rlu) [2, 3]; third, superconductivity coexists with antiferromagnetic order below a relatively high temperature of ∼1.9 K, giving an energy scale accessible to modern high-resolution neutron spectrometers. From the large specific heat and concomitant jump at T_{sc} of $\chi C = 1.2\chi T_{sc}$ ($\chi = 140$ mJ mol^{-1} K^{-2}) [1], it has been suggested that the superconducting ground state evolves out of interactions between heavy quasiparticles at the Fermi surface. Finally, UPd_2Al_3 possesses a set of intriguing physical properties amongst which number a significant uranium moment ∼0.85 μ_B [2–4] and, below T_{sc}, the absence of a Hebel–Slichter peak [5], a T^3 dependence of the nuclear-spin relaxation time, T_1 [6], and a power-law behaviour of the specific heat [7], all of which have prompted suggestions of unconventional superconductivity.

Of the many techniques available for characterizing the spectral magnetic response of this system, neutron inelastic scattering is one of the most powerful, giving information on the electronic and nuclear dynamics over temporal (10^{-13}–10^{-10} s) and spatial (∼400 Å) scales ideally suited to the investigation of both magnetic and superconducting phenomena. A general formalism, based on linear response theory, relating the cross section to the dissipative component of the magnetic susceptibility (Im χ), exists for the scattering of the neutron against stable thermodynamic states [8]. Within its domain of validity, this enables the inference of direct microscopic information on the dynamic evolution of the magnetic quasiparticle–hole excitation spectra in correlated magnetic macrostates. In the superconducting state,

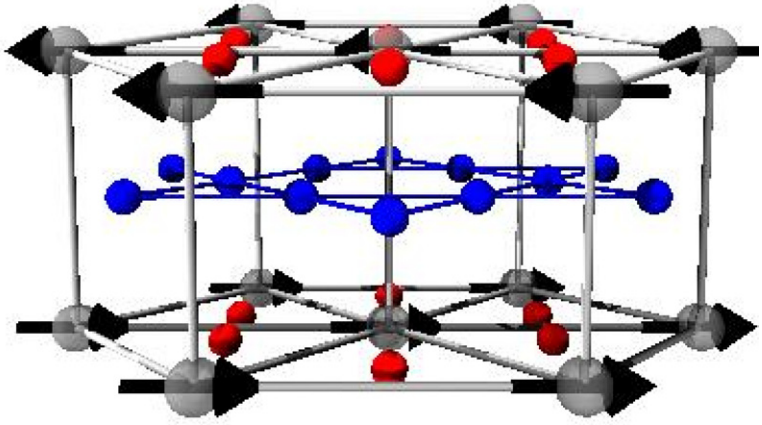

Figure 1. The crystallographic and magnetic structure of UPd_2Al_3. The large circles represent the positions of uranium ions, with the bold arrows marking the relative directions of the magnetic moments. The smaller grey (red) circles in the same planes represent the positions of the palladium ions, while the smallest dark grey (blue) circles, in the intercalating plane, represent the aluminium ions.

the response is modified by the dynamical restrictions imposed by the phase-correlated condensate [9]. In addition to the contribution from the quasiparticle–hole excitations of the normal state, the neutron may also couple directly to the superconducting ground state via transitions associated with excitation/condensation of Cooper pairs. As with the normal state excitations, the amplitude of the response depends on the space–time symmetry of the condensate and, in favourable circumstances, one may observe its signatures through its contribution to the magnetic excitation spectrum. As we shall see, in UPd_2Al_3 this is indeed the case.

Attempts to examine other heavy-fermion superconductors, e.g. UPt_3 [10], URu_2Si_2 [11, 12], UBe_{13} [13], and UNi_2Al_3 [14], by neutron inelastic scattering have all been hampered by the difficulty that the dynamic correlations are weak. In the case of ferromagnetic superconductors such as UGe_2 [15], relevant experiments to access the superconducting ground state would have to be performed under substantial pressures (10–15 kbar) and low temperatures, $T_{sc} \sim 0.2$ K. Similar temperature restrictions in the recently discovered ambient pressure systems, $ZrZn_2$ [16] and URhGe [17], make neutron inelastic scattering experiments difficult from the viewpoint of the temperatures needed as well as the extremely high resolution required to access fluctuations on the scale of T_{sc} ($\sim$20 μeV). These problems are compounded by the intrinsic problem of the separation of nuclear and magnetic contributions to the cross section at the ferromagnetic position. Thus, although inelastic scattering has been observed from these materials, it cannot be correlated in a simple manner with the dynamics of the changing thermodynamic macrostates involved.

It is the specific combination of physical properties that makes a neutron inelastic scattering investigation of the normal-to-superconducting transition in UPd_2Al_3 possible, on account of a dominant *quasi-elastic* contribution to the magnetization autocorrelation function at low energies. This opens an experimental window, via high-resolution neutron inelastic scattering, on the low-energy dynamics that play a key role both in the formation of the antiferromagnetic heavy-fermion state and the simultaneous superconducting ground state.

We start this topical review with a résumé of previous neutron work. We then focus on the investigations close to the magnetic zone centre (section 3.1) before turning to the response observed throughout momentum space (section 3.2). Conclusions are given in section 4.

2. Résumé of previous work using neutron inelastic scattering

The first neutron inelastic scattering work on single crystals was at Risø National Laboratory, in which broad excitations with a strong dispersion along the c^* ([0 0 1]) axis up to ∼8 meV at the magnetic zone boundary (where the full width half maximum (FWHM) is ∼9 meV) were reported [18]. In the basal plane, strongly damped excitations were found, with poles and widths of similar extent, increasing up to ∼4 meV. These studies, carried out with 0.3 meV resolution (FWHM), found no low-energy gap in the excitations at the magnetic zone centre, $\mathbf{Q}_0$, and no change when the material became superconducting. However, since the energy resolution was on the scale of ∼3 K, it is perhaps not surprising that no effect was observed below T_{sc}.

Work on polycrystalline material at the ISIS spallation source by Krimmel *et al* [19] then followed, giving an overview of the inelastic response function up to ∼40 meV. This study gives no clear evidence for a discrete crystal field level scheme, and the principle results of these experiments were that: (a) over the studied range of wavevectors, a broad quasi-elastic contribution was present in the scattering at all measured temperatures with a FWHM of 9.8 meV at $T = 25$ K and 22.8 meV at 150 K; and (b) at $T = 25$ K, a strong maximum in the scattered intensity with an energy transfer ∼2.2 meV at $|\mathbf{Q}| \sim 1$ Å^{-1} was identified.

Experiments on single crystals were made in 1995 by the Tohoku University group using the JRR-3M research reactor (JAERI, Tokai) [20], which motivated higher-resolution experiments at the Institut Laue Langevin, Grenoble (ILL) in 1996 [21]. Around this period, a parallel effort was started by the group at the Advanced Science Research Centre of JAERI in Tokai, Japan [22, 23]. Over the following years, several papers were published, concentrating on the magnetic response in the vicinity of $\mathbf{Q}_0$, the magnetic zone centre, including polarization analysis, and temperature- and field-dependent studies. This has resulted in a disparate literature, masking rather than highlighting the fundamental importance and remarkable degree of agreement between data collected on different samples by independent experimental groups. A point of much interest has been the exploitation of initial results obtained by Metoki *et al* [24] with high-energy resolution techniques to resolve the significant intensity around a second characteristic wavevector, $\mathbf{Q}^* = (1/2\ 0\ 1/2)$; this aspect, investigated in more detail at the ILL and Paul Scherrer Institute (PSI), led to an alternative perspective on the origin of the $\mathbf{Q}_0 = (0\ 0\ 1/2)$ Bragg peaks [25].

In parallel with the experimental program, theoretical efforts have been underway to understand the rather unusual effects reported. Early approaches by Sato *et al* [21, 26] were followed by those of Bernhoeft *et al* [27–31] which exploited the changes in wavevector and energy dependences of the neutron inelastic scattering amplitude below T_{sc} to infer the symmetry of the energy gap in an analysis based on the role of the phase coherence intrinsic to the superconducting macrostate. More recently, Sato *et al* [32] have published an alternative interpretation of the *same* data, building on some aspects of the interpretation given in [27–31]. Whilst further work [33] on tunnelling into carefully prepared films supports the interpretations drawn in [27–31], various other conclusions on the energy gap symmetry, together with more general remarks about the potential driving the superconductivity [32–36], have also appeared.

In view of the general interest generated by the data from these experiments, which arises from their rich information content with respect to the superconducting energy gap symmetry and magnitude, further experiments using cold and thermal three-axis spectrometers have recently been performed. This review provides a comprehensive coverage of the current experimental situation. Important new data are presented, mainly in the form of extensive surveys in energy–momentum space under a wide range of experimental conditions. All comparable data presented are consistent between experiments performed on independent samples at JAERI, ILL, and PSI.

To avoid confounding the data, which stand alone, with interpretations, the analytic reduction of the results is deferred to the following paper [37]. It is hoped that the combination of papers may stimulate an interaction between theoretical modelling and further experiments in developing an understanding of the antiferromagnetic superconducting state.

3. Experimental results

The experiments have been performed on two different samples at JEARI, and the ILL and PSI, respectively. Experimental details can be found in the original papers, although some important instrumental parameters are given in the figure captions. All data have been taken in neutron energy loss. Since almost all the features in the magnetic response function of UPd_2Al_3 are broad both in energy and momentum space, the instrumental resolution (especially when using cold-source instruments such as IN14 at the ILL) has been adjusted so that it is not a determining factor. The resolution is also marked on most of the figures.

The crystals were grown using the Czochralski method from a melt of high-purity elements with a nominal composition of $UPd_{2.02}Al_{3.03}$ [38, 39]. They have a typical mass of ∼2.5 g, are cylindrical in shape, and show a mosaic spread of about 1°. Both samples exhibit a superconducting transition at ∼1.9 K.

3.1. Overview of the effects around the magnetic zone centre $\boldsymbol{Q}_0 = (0\ 0\ 1/2)$

Data on the magnetization dynamics at, and close to, the magnetic zone centre along the c^* direction are summarized in figures 2–5. In figure 2(a), an overview of the temperature evolution at $\mathbf{Q}_0$ is given. At high temperatures, in the paramagnetic state, the response is, within the experimental energy resolution of 0.09 meV (FWHM), quasi-elastic. Inside the antiferromagnetically ordered state, quasi-elastic scattering remains present. In the temperature range from about 2 to 7 K, the strength of the quasi-elastic intensity scales approximately with k_BT, indicating that the susceptibility is more or less temperature independent. In addition to this quasi-elastic response, on cooling, a distinct, albeit broad, inelastic feature (grey (green) arc)—described as a spin wave [18] or exciton mode [32]—appears. At $\mathbf{Q}_0$, for temperatures below 2.5 K, this latter mode is observed at an energy transfer of $E \sim k_BT_N$ (1.5 meV) with a width of ∼0.4 meV (FWHM), which is much greater than the energy resolution of the spectrometer. This broad feature remains unchanged when passing into the superconducting phase down to the lowest temperatures measured (0.15 K). In contrast, below T_{sc} a change in profile at low energies occurs, with the quasi-elastic response being replaced by a distinct excitation (diffuse light grey (orange) area in the lower left-hand corner) apparently associated with the superconducting state.

In figure 2(b) some of the data used to construct figure 1(a) are shown. The arrows indicate, without any detailed modelling, the approximate intensity maxima of the inelastic features discussed above. The solid line is a smooth fit to 1.75 K data (black squares) and this line has been scaled by the Bose factor (with a constant background subtracted) and overlaid over the 0.15 K (open circles) and 2.5 K (open diamonds) data. At 0.15 K, this procedure clearly fails to reproduce the data, indicating that there is a significant *change* in the low-energy response. This change in the response is further emphasized in figure 3. In figure 3(a) we show the measured intensity at an energy transfer of 0.38 meV. The large peak at T_N is associated with the expected maximum in susceptibility at the antiferromagnetic wavevector $\mathbf{Q}_0$. On lowering the temperature, the intensity first decreases below T_N, but increases again on entering the superconducting state. In figure 3(b) we show q-scans through the response at an energy transfer of 0.4 meV, indicating that the spatial extent of the response below T_{sc} is similar to that above. The widths correspond to a spatial extent along the c^* axis of ∼100 Å.

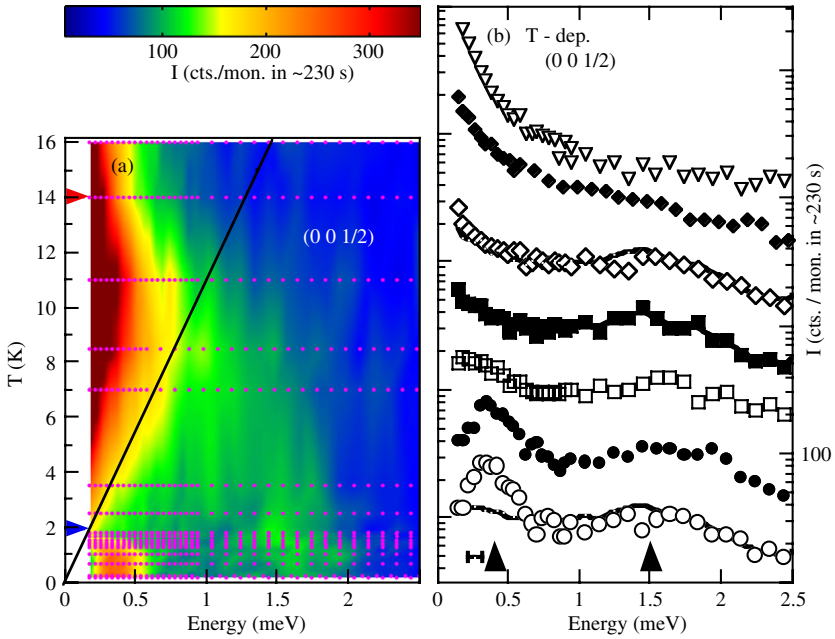

Figure 2. (a) Contour plot of the intensity at $\mathbf{Q}_0 = (0\ 0\ 1/2)$ as a function of temperature and energy transfer. Marked on the plot are the energies of the characteristic temperatures T_{sc} and T_N and the line $E = k_B T$ to indicate the approximate division between thermal-and quantum-induced fluctuations. In this and succeeding contour maps, the dots indicate the data collection points used in construction of the map. (b) The inelastic response at $\mathbf{Q}_0$ for (from bottom to top) $T = 0.15$, 1.0, 1.5, 1.75, 2.5, 7 and 14 K. Note the alternating logarithmic intensity scales displaced by half a decade, as indicated on the left- and right-hand ordinates; open symbols refer to left- and closed symbols to right-hand scales, respectively. The solid lines, as well as the vertical arrows, are discussed in the text. The horizontal bar indicates the instrumental resolution. Except when indicated, the statistical error corresponds to the size of the symbols. Data taken at ILL on IN14 with $k_f = 1.15$ Å^{-1}. In this and all succeeding figures, data are taken in neutron energy loss. The left-hand figure and some of the data have been published previously [27–32].

Given the strong, qualitative change in character of the low-energy response on passing below T_{sc}, it is important to establish the nature of the peak occurring for $T < T_{sc}$. Careful polarization analysis has been carried out at $\mathbf{Q}_0$, and we refer to figure 2 of our previous publication [27] for details. These results establish that the entire dynamical response for 0.15 K $< T <$ 10 K is predominately spin reversing (i.e. time asymmetric), *transversely polarized* to the magnetic moment and, taken with the $\mathbf{Q} \times (\mathbf{Q} \times \mathbf{M})$ selection of the neutron dipole cross section, polarized in the hexagonal basal plane. A longitudinal contribution, characteristic of modes polarized parallel to the bulk moment, is not observed below 10 K. These results eliminate scenarios in which the quasi-elastic response of the normal state is destroyed on entering the superconducting phase and replaced by, for example, a phononic contribution.

The low-energy inelastic feature is not only progressively quenched on heating at zero field, figure 2, but also, at $T = 0.4$ K, under an applied magnetic field [23]. The collapse in both position and intensity of the low-energy inelastic feature around B_{c2} (=3.6 T) is strong support for the low-energy inelastic signal being related to the development of superconductivity.

We now turn to the form of the response in the immediate vicinity of $\mathbf{Q}_0$. The dispersion parallel to the hexagonal axis in the vicinity of $\mathbf{Q}_0$ is given in figures 4 and 5. Comparing the

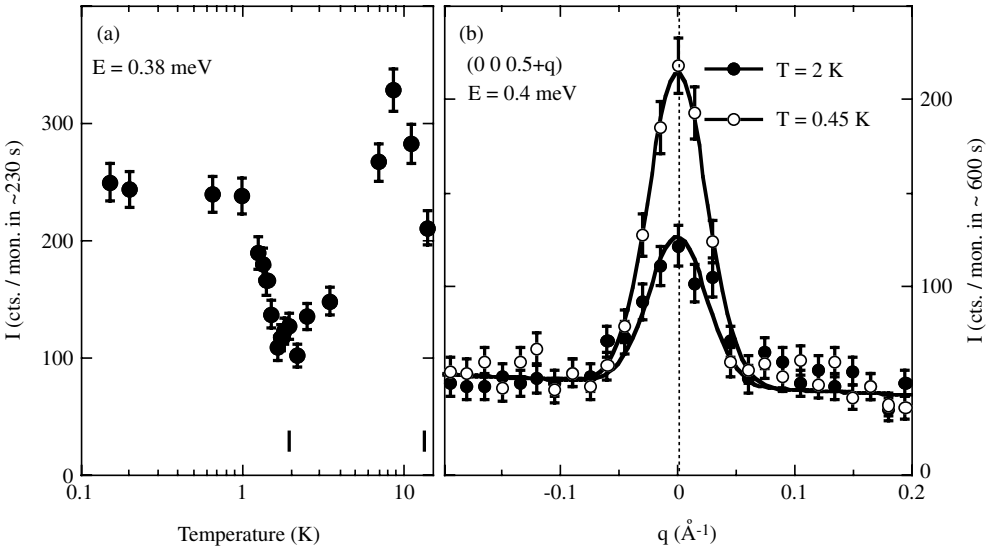

Figure 3. (a) Neutron intensity at $\mathbf{Q}_0$ and energy transfer of 0.4 meV as a function of temperature. Data taken at ILL on IN14 with $k_f = 1.15$ Å^{-1}. Vertical bars mark the transition temperatures T_{sc} and T_N. (b) Neutron intensities as a function of q_l along the $\boldsymbol{c}^*$ axis taken at constant energy transfer of 0.4 meV in both the normal and superconducting states. Data taken at JAERI with incident wavevector fixed at $k_i = 1.5$ Å^{-1} with a corresponding energy resolution of ~0.2 meV (FWHM).

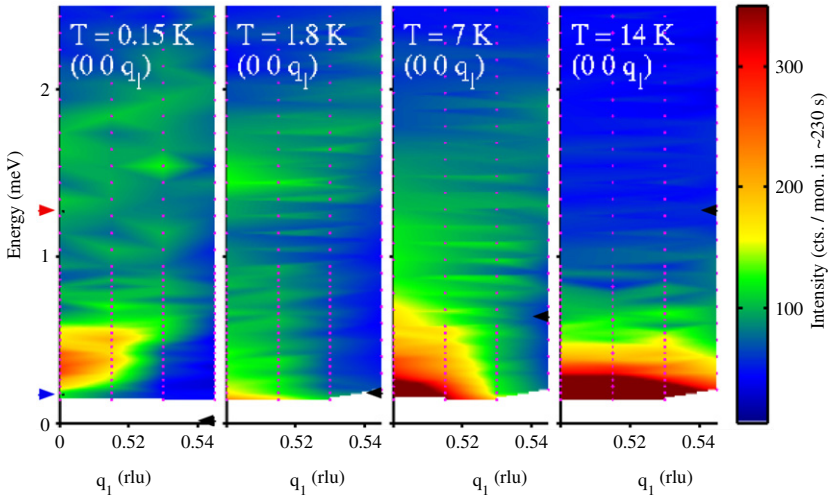

Figure 4. Contour plots of the intensity at four temperatures (marked) as a function of $\mathbf{q} = (0\ 0\ q_l)$ and energy transfer. On the energy scale, dark arrows (red and blue) on the left-hand side, mark the energies corresponding to the antiferromagnetic, T_N, and the superconducting, T_{sc}, transitions with the sample temperature, T, indicated by dark (black) arrows on the right-hand side on each panel. Data taken at ILL on IN14 with $k_f = 1.15$ Å^{-1}. The figure has been published previously [27].

responses at 14 and 7 K, not only does the high-energy 'spin-wave-like' feature develop, but the quasi-elastic scattering appears more localized in momentum space. At $T = 1.8$ K ($\sim T_{sc}$), both the low- and high-energy features are apparent. The former has a quasi-elastic lineshape

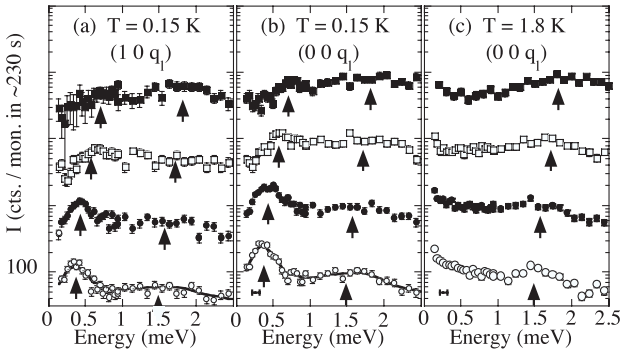

Figure 5. Dispersion of the inelastic response for (a) $\mathbf{Q} = (1\ 0\ q_l)$ at 0.15 K, (b) $\mathbf{Q} = (0\ 0\ q_l)$ at 0.15 K, and (c) $\mathbf{Q} = (0\ 0\ q_l)$ at 1.8 K with (from bottom to top) $q_l = 0.500$, 0.515, 0.530, 0.545. Note that the logarithmic vertical scale and the zero level of successive scans are displaced by one decade for clarity. The solid lines are discussed in the text. The horizontal bar indicates the instrumental resolution. Except when indicated, the statistical error corresponds to the size of the symbols. Data taken at ILL on IN14 with $k_f = 1.15$ Å^{-1}.

and exhibits a marked decay in amplitude with increasing wavevector along q_l. On this scale, close to $\mathbf{Q}_0$, the latter (the inelastic mode) retains its amplitude and form. For the lowest temperature (0.15 K), both the spin wave and excitation associated with the superconducting state are inelastic, and this is maintained on moving away from $\mathbf{Q}_0$ with, once again, a rapid reduction in intensity of the latter excitation associated with the superconducting state. Figure 5 gives a more quantitative illustration of the response around $\mathbf{Q}_0$, showing the rapid fall-off of the intensity of the low-energy excitation associated with the superconducting state, contrasted with the small changes in the spin-wave response over this small q range. In addition, the solid line shown in the (1 0 1/2) scan in figure 5(a) is a smooth fit to the scan at (0 0 1/2) of figure 5(b) reduced by the factor 2.2 (with a constant background subtracted), as expected from the uranium form factor. This shows that the whole response arises from a magnetic density of similar spatial extent.

At comparable temperatures, the thermal evolution in the normal state in the hexagonal plane (q_h 0 1/2) and along the hexagonal axis (0 0 q_l) are given in the left-and right-hand panels of figure 6. The upper panels suggest an almost isotropic quasi-elastic response for $T \sim T_N$ over this q range, but that it becomes more localized in reciprocal space (i.e. the correlations become longer in real space) as the temperature is lowered. At the same time, the inelastic (spin wave or exciton) feature around 1.5 meV, which is not evident in the paramagnetic state, continues unabated to at least $q_h \sim 0.08$ rlu.

The neutron inelastic scattering spectra of figures 2–5 clearly highlight the change in the low-energy response on passing below T_{sc} with the *inelastic* feature associated with the superconducting state being *qualitatively* different from the quasi-elastic signal in the normal state. Thus, whilst both are approximately constant in spatial extent, remain transversely polarized, and strongly focused around $\mathbf{Q}_0$, the internal dynamics rearrange with the evolution of an excitation gap in the magnetic response. However, in contrast with the thermally excited quasi-elastic scattering of the normal state, this emergent, inelastic response lies significantly above $k_B T$. It exhibits a strong dispersion in the vicinity of $\mathbf{Q}_0$, both along the hexagonal axis and in the basal plane.

Despite the dramatic changes in the low-energy excitation spectrum in the superconducting phase when below $\sim T_{sc}/2$, the spin wave at 1.5 meV differs little in its presentation from that

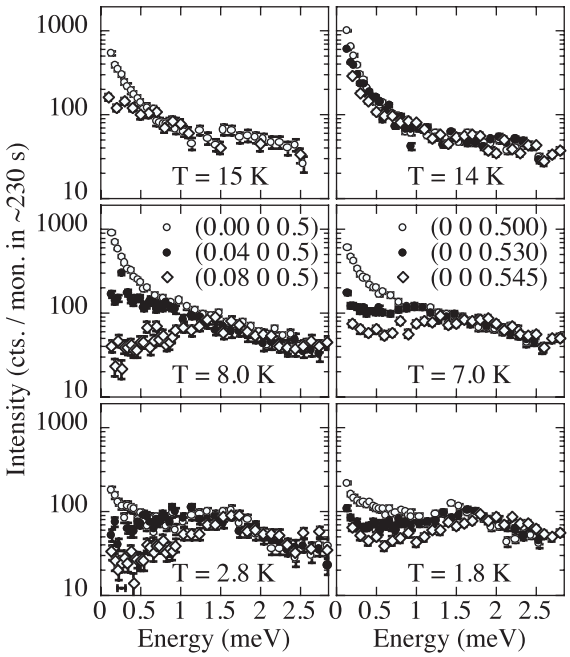

Figure 6. Comparison of the scattering in the hexagonal plane (q_h 0 1/2) (left) and along the hexagonal c^* axis (0 0 q_l) (right) at different temperatures in the normal state. Note (i) the logarithmic vertical scale, (ii) the different steps in reciprocal space (a reciprocal lattice unit corresponds to $a^* = 1.355$ Å^{-1} and $c^* = 1.500$ Å^{-1} along the two axes) and (iii) that the intermediate data set at (0.04 0 0.5) has not been measured at $T = 15$ K. Data taken at ILL on IN14 with $k_f = 1.15$ Å^{-1}.

in the normal state; see figures 2, 4 and 5. Models based on the thermal evolution of this feature depend critically on the assumptions in a given scenario and can lead to quantitative changes in the inferred energy position and width below T_{sc} [32]. Such details, however, are *not* robust features of the data, but depend *sensitively* on the modelling. Any meaningful parameterization must include the evident dispersion and fit all data under a given thermodynamic condition simultaneously. For this reason, in this review, we do not enter into detailed modelling, and we use arrows in figures 2 and 5 to indicate approximate maxima of the inelastic features.

To summarize, the magnetic response close to $\mathbf{Q}_0$ comprises: (i) a quasi-elastic response for all temperatures $T > \sim T_{sc}$, (ii) an inelastic (spin-wave or exciton) response in both the normal and superconducting antiferromagnetically ordered states for $T < T_N$, and (iii) the dramatic growth of an inelastic feature at energies ~0.4 meV in the superconducting phase for temperatures below T_{sc}.

3.2. The response across the Brillouin zone

The response across the Brillouin zone well below T_{sc} for energy transfers up to 4 meV is shown in figure 7. The strong localization of scattering around $\mathbf{Q}_0$ is evident, and the left-hand and central panels illustrate the dispersion of the spin-wave-like excitation in the (0 0 q_l) and (q_h 0 1/2) directions, respectively. In contrast, as shown in the central and right-hand panels, the response in the basal plane (q_h 0 1/2) is complex in form, having a subsidiary maximum at the position $\mathbf{Q}^* = (1/2\ 0\ 1/2)$ as first reported by Metoki *et al* [24]. The broad intensity

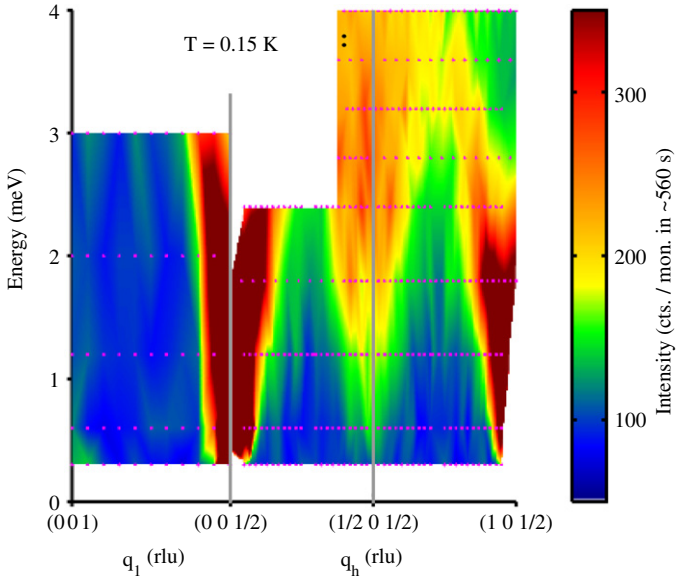

Figure 7. Contour map at 0.15 K showing the response at relatively low-energy transfer across the Brillouin zone in the (0 0 q_l) direction (left-hand panel) and the (q_h 0 1/2) direction (right-hand panel). The magnetic zone centres ($\mathbf{Q}_0$) are (0 0 1/2) and (1 0 1/2). The abscissa are scaled to accommodate the different a and c axis lattice parameters. The grey-scale (colour) scheme, designed to highlight the additional intensity around $\mathbf{Q}^* = (1\ 0\ 1/2)$, leads to a saturation close to $\mathbf{Q}_0$. The cross section at the smallest energy transfers is inaccessible due to incoherent elastic scattering and, at $\mathbf{Q}_0 = (0\ 0\ 1/2)$, due to the antiferromagnetic Bragg peak. Data taken at ILL on IN14 with $k_f = 1.3$ Å^{-1}.

maximum is associated with a range of wavevectors around $\mathbf{Q}^*$ and, at this temperature, appears at an energy transfer of ∼3 meV. This is further illustrated and extended to higher energies in the right-hand panel of figure 8 for data taken at 1.5 K. Under the same conditions, the left-hand panel illustrates the dispersion, increase in width, and decay into weak diffuse scattering of the spin-wave excitation in the (0 0 q_l) direction. This is in agreement with the original measurements of [18] at these higher energies.

Away from $\mathbf{Q}_0$, the dispersive spin-wave-like mode decays into weak space–time correlations. As a model independent approach, which implicitly ignores all coupling and damping effects, figure 9 gives the intensity maxima in the intermediate q-region as observed at $T = 2$ K in the form of a dispersion relation. At small values of q_l and q_h, the distinct components are resolved (given as open circles), while above ∼0.05 rlu away from $\mathbf{Q}_0$, as indicated by the filled circles, the quasi-elastic response collapses, leaving a distinct dispersive mode, which has a stiffness differing by ∼50% in the two directions.

Previous work found the cross section for modes propagating in the basal plane to be poorly defined in momentum and energy transfer at all temperatures below T_N [18, 19, 21–24]. The thermal evolution in the normal state of the enhanced, broad response at $\mathbf{Q}^*$, which has a typical energy scale of 35 K, is shown in the contour plots of figure 10 at 2.5, 12 and 20 K. For $|\mathbf{Q}| \sim |\mathbf{Q}^*| \sim 1$ Å^{-1}, an earlier paper by Krimmel *et al* [19] using a time-of-flight technique and polycrystalline material noted an enhanced response with a typical energy of ∼2.2 meV and width of 0.75 meV (FWHM) above T_N, at 25 K. Note that any such response at $\mathbf{Q}^*$ appears amplified in a polycrystalline sample, as several positions in the basal plane, all displaced by $q = |q_h| = 1/2$ around the $\mathbf{Q}_0 = (0\ 0\ 1/2)$ position, contribute to the observed signal.

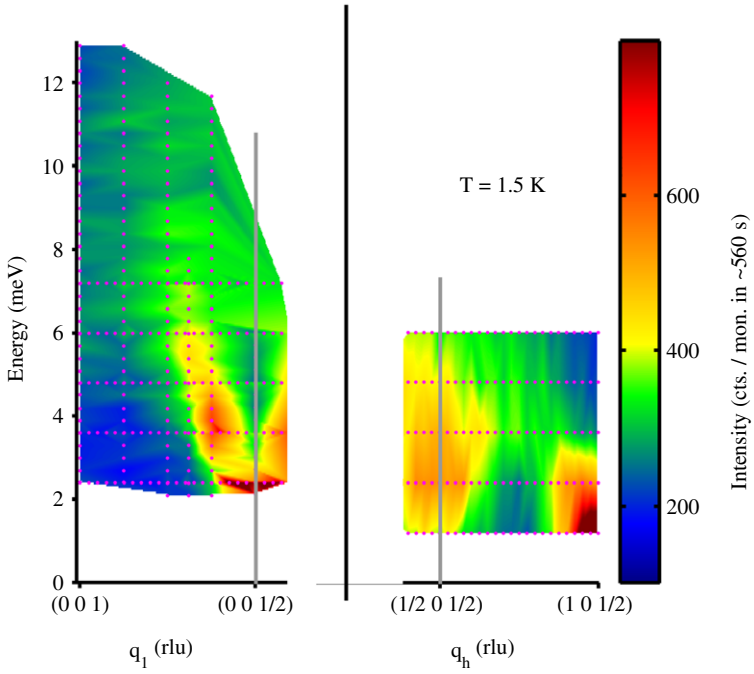

Figure 8. Left- and right-hand panels give contour plots of the intensity at 1.5 K in the (0 0 q_l) and (q_h 0 0) directions across the zone as determined using the thermal three-axis spectrometer IN8 at ILL with $k_f = 2.662$ Å^{-1}. The energy resolution is ∼1 meV (FWHM).

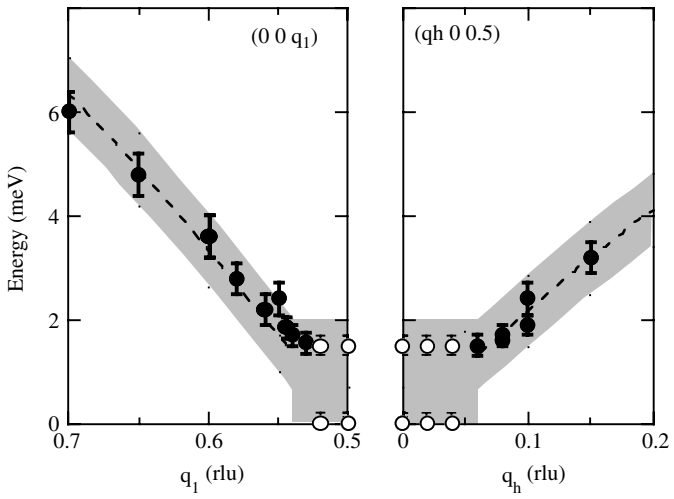

Figure 9. Plot of intensity maxima as a function of q around $\mathbf{Q}_0$ with $T \sim 2$ K. The closed symbols indicate data from scans in which a single maximum is observed. Open symbols indicate regions where two features are observed in energy scans. The grey area of ±0.7 meV around $\mathbf{Q}_0$ indicates the region over which the intensity has at least 50% of its peak value. The dashed line corresponds to a stiffness of 14.6 meV Å in the $\boldsymbol{c}^*$ direction (left-hand panel) and 10.5 meV Å in the basal plane (right-hand panel). The abscissa are scaled to accommodate the different a- and c-axis lattice parameters.

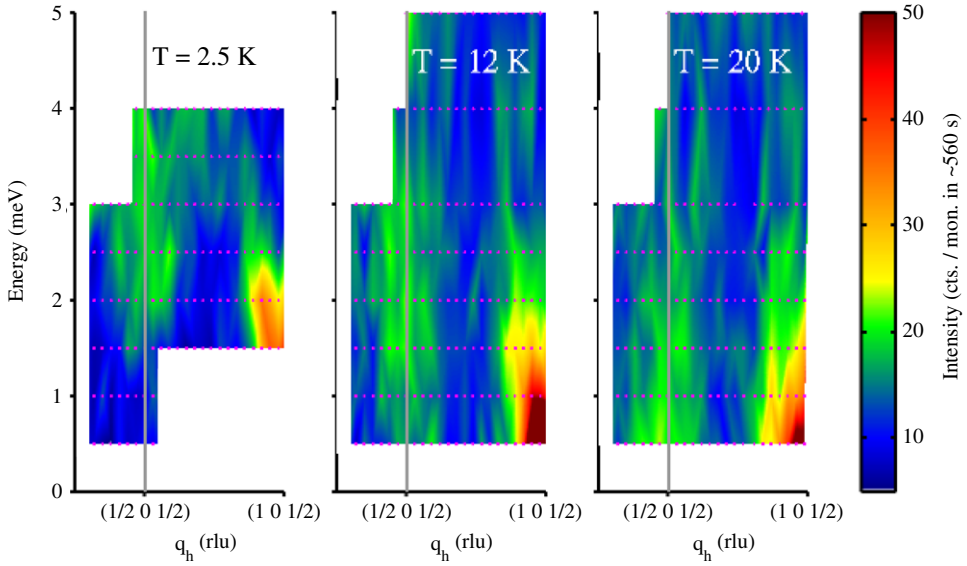

Figure 10. Inelastic response across the zone from (1/2 0 1/2) to (1 0 1/2) at three temperatures. The intensity recorded at (1 0 1/2) marks an equivalent $\mathbf{Q}_0$ position. Data taken at PSI on TASP with $k_f = 1.5$ Å^{-1}.

In figure 11 the left-hand panel extends the observations to higher temperatures and energy transfer. In the paramagnetic regime, a broad response is present at both $\mathbf{Q}_0$ and $\mathbf{Q}^*$. Additionally, as the right-hand panel in figure 11 shows, at and below T_N for the smallest energy transfer measured (∼0.2 meV), there is an enhancement at $\mathbf{Q}_0$ of the low-energy (long-time correlations) excitation, with no similar signal at $\mathbf{Q}^*$. Figure 12 emphasizes the difference in response at 0.2 K between $\mathbf{Q}_0$ and $\mathbf{Q}^*$ in the superconducting state: at $\mathbf{Q}^*$ there is no observable response at low energies in the superconducting state, in sharp contrast with the situation around $\mathbf{Q}_0$. Thus, for low temperatures, the intensity at the $\mathbf{Q}^*$ position has no quasi-elastic contribution and exhibits no observable change as the temperature is lowered through T_{sc}. This lack of a low-energy response in the vicinity of $\mathbf{Q}^*$ in UPd_2Al_3 may be contrasted with the case of UNi_2Al_3, which orders at an incommensurate wavevector close to $\mathbf{Q}^*$ at $(1/2 \pm 0.11\ 0\ 1/2)$ [14, 40].

In summary, at $\mathbf{Q}^*$ and low temperature, there is an inelastic response that is broad in both energy and wavevector transfer. However, there is no quasi-elastic feature at any temperature in the normal antiferromagnetic phase or low-energy inelastic response analogous to that seen around $\mathbf{Q}_0$ at temperatures well below T_{sc}.

4. Conclusion

Previous publications [21–32] have concentrated on the response around $\mathbf{Q}_0$ and its temperature dependence. This has also been the main focus of theoretical efforts [25–32, 34–36]. The present paper affords new insights by extensive and detailed mapping through the Brillouin zone of the temperature-dependent response from well below T_{sc} to $\sim 5T_N$. The maps, which encompass the two major symmetry directions of the reciprocal lattice (parallel and perpendicular to the hexagonal axis), show that the magnetic response in UPd_2Al_3 is strongly structured in both momentum and energy.

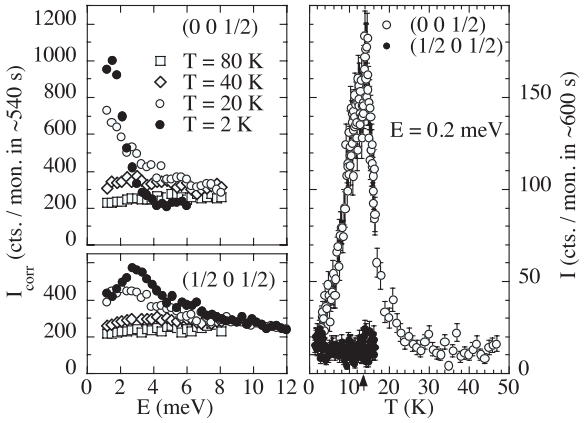

Figure 11. Left-hand panels: constant q-scans at $\mathbf{Q}_0$ and $\mathbf{Q}^*$ at different temperatures. The observed intensity has been corrected by the Bose factor at all temperatures, assuming a constant background of 200 cts. The data below 1 meV have been suppressed, since they fall within the (elastic) resolution window of the spectrometer. Data taken on IN8 with $k_f = 2.662$ Å^{-1}. Right-hand panel: temperature dependence of the low-energy response at the two positions $\mathbf{Q}_0$ and $\mathbf{Q}^*$ taken at 0.2 meV energy transfer. Data taken at PSI on TASP with $k_f = 1.15$ Å^{-1}.

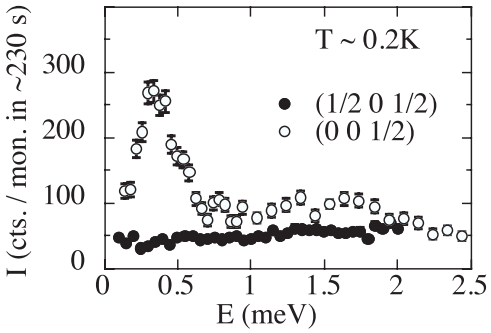

Figure 12. Constant q-scans at $\mathbf{Q}_0$ and $\mathbf{Q}^*$ taken below T_{sc}. Data taken at ILL on IN14 with $k_f = 1.15$ Å^{-1}.

In addition to the rich energy structured response in the vicinity of $\mathbf{Q}_0$, which has been discussed in [21–31], there is a secondary maximum at the wavevector $\mathbf{Q}^*$ which persists from 150 mK in the antiferromagnetic-superconducting state to above T_N in the paramagnetic phase, as illustrated in figures 7–12. While the detailed implications for thermodynamic properties of having such multiple maxima in the momentum space wave remains unclear, they appear as a common theme in strongly correlated electronic systems [10–14], and in the present case it has been proposed that the nominally ordered state in UPd_2Al_3 remains dynamic in nature on account of the $\mathbf{Q}^*$ mode [25].

The task of understanding a coherent antiferromagnetic-superconducting ground state remains a major challenge in condensed matter physics. In the interim, we hope that the rich and robust nature of the data on UPd_2Al_3 presented here will stimulate further experiments and discoveries of other model systems. In the following paper [37], we complement these studies with a critical appraisal of the assumptions, scope and limits inherent in analyses of inelastic neutron scattering data and the modelling of the magnetic response function.

Acknowledgments

We thank all colleagues who have helped this work, in particular the critique of E Blackburn, A Kreyssig and O Stockert is appreciated. Both GHL and NB would like to thank the Director and staff of the Advanced Science Research Centre, JAERI, for warm hospitality during visits that have advanced this collaboration. AH thanks colleagues at IFP, Technische Universität, Dresden, and at the Max-Planck-Institut für chemische Physik fester Stoffe, Dresden (Germany) for hospitality during his visit. The neutron inelastic scattering experiments have been performed at the Institut Laue Langevin (France), JAERI (Japan) and the SINQ source at PSI (Switzerland).

References

[1] Geibel C, Schank C, Thies S, Kitazawa H, Bredl C D, Bohm A, Rau M, Grauel A, Caspary R, Helfrich R, Ahlheim U, Weber G and Steglich F 1991 *Z. Phys.* B **84** 1
[2] Krimmel A, Fischer P, Roessli B, Maletta H, Geibel C, Schank C, Grauel A, Loidl A and Steglich F 1992 *Z. Phys.* B **86** 161
[3] Kita H, Dönni A, Endoh Y, Kakurai K, Sato N and Komatsubara T 1994 *J. Phys. Soc. Japan* **63** 726
[4] Paolasini L, Paixão J A, Lander G H, Burlet P, Sato N and Komatsubara T 1994 *Phys. Rev.* B **49** 7072
[5] Kyogaku M, Kitaoka Y, Asayama K, Geibel C, Schank C and Steglich F 1993 *J. Phys. Soc. Japan* **62** 4016
Kohori Y and Kohara T 1994 *Physica* B **199/200** 135
[6] Matsuda K, Kohori Y and Kohara T 1997 *Phys. Rev.* B **55** 15223
[7] Caspary R, Hellmann P, Keller M, Sparn G, Wassilew C, Köhler R, Geibel C, Schank C, Steglich F and Phillips N E 1993 *Phys. Rev. Lett.* **71** 2146
[8] Lovesey S W 1984 *Theory of Neutron Scattering from Condensed Matter* (Oxford: Oxford University Press)
[9] Schrieffer J R 1964 *Theory of Superconductivity* (New York: Benjamin-Cummings)
[10] Aeppli G, Bishop D, Broholm C, Bucher E, Siemensmeyer K, Steiner M and Stüsser N 1989 *Phys. Rev. Lett.* **63** 676
Isaacs E D, Zschack P, Broholm C L, Burns C, Aeppli G, Ramirez A P, Palstra T T M, Erwin R W, Stücheli N and Bucher E 1995 *Phys. Rev. Lett.* **75** 1178
[11] Broholm C, Kjems J K, Buyers W J L, Mathews P T, Palstra T T M, Menovsky A A and Mydosh J A 1987 *Phys. Rev. Lett.* **58** 1467
Broholm C, Kjems J K, Buyers W J L, Mathews P T, Palstra T T M, Menovsky A A and Mydosh J A 1991 *Phys. Rev.* B **43** 12809
[12] Fåk B, Vettier C, Flouquet J, Boudarot F, Raymond S, Vernière A, Lejay P, Boutrouille Ph, Bernhoeft N, Bramwell S T, Fisher R A and Phillips N E 1996 *J. Magn. Magn. Mater.* **154** 339
[13] Coad S, Hiess A, McMorrow D, Lander G H, Aeppli G, Fisk Z, Stewart G, Hayden S and Mook H 2000 *Physica* B **276–278** 764
Hiess A, Heffner R H, Sonier J E, Lander G H, Smith J L and Cooley J 2002 *Phys. Rev.* B **66** 064531
[14] Aso N, Roessli B, Bernhoeft N, Calemczuk R, Sato N K, Endoh Y, Komatsubara T, Hiess A, Lander G H and Kadowaki H 2000 *Phys. Rev.* B **61** R11867
Gaulin B D, Mao M, Wiebe C R, Qiu Y, Shapiro S M, Broholm C, Lee S-H and Garrett J D 2002 *Phys. Rev.* B **66** 174520
[15] Saxena S S, Agarwal P, Ahilan K, Grosche F M, Haselwinner R K W, Steiner M J, Pugh E, Walker I R, Julian S R, Monthoux P, Lonzarich G G, Huxley A, Sheikin I, Braithwaite D and Flouquet J 2000 *Nature* **406** 507
[16] Pfleiderer C, Uhlarz M, Hayden S M, Vollmer R, von Löhneysen H, Lonzarich G G and Bernhoeft N 2001 *Nature* **412** 58
[17] Aoki D, Huxley A, Ressouche E, Braithwaite D, Flouquet J, Brison J-P, L'hotel E and Paulsen C 2001 *Nature* **413** 613
[18] Petersen T, Mason T E, Aeplli G, Ramirez A P, Bucher E and Kleinman R N 1994 *Physics* B **199/200** 151
Mason T E and Aeppli G 1997 *Mat.-Fys. Med. (Copenhagen)* **45** 231
[19] Krimmel A, Loidl A, Eccleston R, Geibel C and Steglich F 1996 *J. Phys.: Condens. Matter* **8** 1677
[20] Aso N 1997 *PhD Thesis* Tohoku University, unpublished
[21] Sato N, Aso N, Lander G H, Roessli B, Komatsubara T and Endoh Y 1997 *J. Phys. Soc. Japan* **66** 1884–7
Sato N, Aso N, Lander G H, Roessli B, Komatsubara T and Endoh Y 1997 *J. Phys. Soc. Japan* **66** 2981
[22] Metoki N, Haga Y, Koike Y, Aso N and Onuki Y 1997 *J. Phys. Soc. Japan* **66** 2560

[23] Metoki N, Haga Y, Koike Y and Onuki Y 1998 *Phys. Rev. Lett.* **80** 5417
[24] Metoki N, Koike Y, Haga Y and Onuki Y 1999 *Physica* B **259–261** 660
[25] Bernhoeft N 2001 *J. Phys. Soc. Japan* **70** (Suppl. A) 7
[26] Sato N, Aso N, Roessli B, Lander G H, Komatsubara T, Endoh Y and Sakai O 1998 *J. Alloys Compounds* **271–273** 433
[27] Bernhoeft N, Sato N, Roessli B, Aso N, Hiess A, Lander G H, Endoh Y and Komatsubara T 1998 *Phys. Rev. Lett.* **81** 4244
[28] Bernhoeft N, Roessli B, Sato N, Aso N, Hiess A, Lander G H, Endoh Y and Komatsubara T 1999 *Physica* B **259–261** 614
[29] Bernhoeft N, Roessli B, Sato N, Aso N, Hiess A, Lander G H, Endoh Y and Komatsubara T 2000 *Physica* B **281/282** 993
[30] Bernhoeft N 1999 *Electron Correlations and Materials Properties* ed A Gonis, N Kioussis and M Ciftan (New York: Kluwer Academic, Plenum) p 137
[31] Bernhoeft N 2000 *Eur. Phys. J.* B **13** 685
[32] Sato N K, Aso N, Miyake K, Shiina R, Thalmeier P, Varelogiannis G, Geibel C, Steglich F, Fulde P and Komatsubara T 2001 *Nature* **410** 340
Sato N K 2003 *Physica* C **388/389** 533
[33] Jourdan M, Huth M and Adrian H 1999 *Nature* **398** 47
Huth M, Jourdan M and Adrian H 2000 *Eur. Phys. J.* B **13** 695
[34] Miyake K and Sato N K 2001 *Phys. Rev.* B **63** 052508
[35] Thalmeier P 2002 *Eur. Phys. J.* B **27** 29
McHale P, Fulde P and Thalmeier P 2004 *Phys. Rev.* B **70** 014513
[36] Oppeneer P M and Varelogiannis G 2003 *Phys. Rev.* B **68** 214512
[37] Bernhoeft N, Hiess A, Metoki N, Lander G H and Roessli B 2006 *J. Phys.: Condens. Matter* **18** 5961
[38] Sato N, Sakon T, Takeda N, Komatsubara T, Geibel C and Steglich F 1992 *J. Phys. Soc. Japan* **61** 32
[39] Haga Y, Yamamoto E, Inada Y, Aoki D, Tenya K, Ikeda M, Sakakibara T and Onuki Y 1996 *J. Phys. Soc. Japan* **65** 3646
[40] Lussier J G, Mao M, Schröder A, Garrett J D, Gaulin B D, Shapiro S M and Buyers W J L 1997 *Phys. Rev.* B **56** 11749